

# Strong pinning at high growth rates in Rare Earth Barium Cuprate (REBCO) superconductor films grown with liquid-assisted processing (LAP) during pulsed laser deposition

J. Feighan<sup>1</sup>, M.H. Lai<sup>1</sup>, A. Kursumovic<sup>1</sup>, D. Zhang<sup>2</sup>, H. Wang<sup>2</sup>, J.H. Lee<sup>3</sup>, S Moon<sup>3</sup>,  
J.L. MacManus-Driscoll<sup>1</sup>

1: Department of Materials Science & Metallurgy, University of Cambridge, 27 Charles Babbage Road, Cambridge, CB3 0FS, United Kingdom

2: School of Materials Engineering, Purdue University, 701 West Stadium Avenue, West Lafayette, IN 47907-2045, USA

3: SuNAM, 52 Seungnyang-gil, Wongok-myeon, Anseong-si, Gyeonggi-do 17554, South Korea

## Abstract

We present a simple liquid assisted processing (LAP) method, to be used *in-situ* during pulsed laser deposition growth to give both rapid growth rates (50 Hz deposition leading to >250 nm/min with a single plume) *and* strong pinning (improved x 5-10 over plain standard YBCO films grown at similar rates). Achieving these two important features simultaneously has been a serious bottleneck to date. LAP enhances the kinetics of the film growth so that good crystalline perfection can be achieved at up to 60 x faster growth rates than normal, while also enabling artificial pinning centres to be self-assembled into fine nanocolumns. In addition, LAP allows for RE mixing (80% of Y with 20% of Yb, Sm, or Yb+Sm), creating effective point-like disorder within the REBCO lattice and which leads to strongly improved pinning at 30 K and below. Overall, LAP is a simple method which could be adopted by other *in-situ* physical or vapour deposition methods (i.e PLD, MOCVD, evaporation, etc) to significantly enhance both growth rate and performance.

## Introduction

(Rare-Earth)Ba<sub>2</sub>Cu<sub>3</sub>O<sub>7-x</sub> or REBCO coated conductors have the potential to revolutionise multiple power and high field magnet applications [1] [2]. However, despite great advances in coated conductor technology over the past 25 years, achieving high in-field performance and low cost simultaneously still remains challenging [3]. Of particular importance is mid-field (3-10 T) applications working at low temperatures (20-30 K), including generators for wind turbines, motors, etc. Standard vapour-grown REBCO films can deliver good performance in this region but growth rates are relatively slow and yields are uncertain. A reliable method for fast growth, with high yield, giving strong pinning is needed. The higher the supersaturation the process, the better in terms of yield and uniformity, and PLD is the best process in that regard. If speeds of PLD could be increased, while maintaining good performance, then costs will come down. The question is how to achieve this goal.

Higher speed growth can be achieved via the use of liquid-assisted methods owing to the faster growth kinetics. The first liquid growth method used to produce REBCO was via a method called liquid phase epitaxy (LPE) [4] [5] [6], initially developed by the semiconductor industry to grow III-V, II-VI and IV-VI compounds for various device applications. e.g. the GaAs/GaAlAs double-heterostructure laser diode [7]. When used to grow REBCO, it was shown to enable growth rates at least x 50 higher than standard [8]. However, LPE is not an industrially practical process owing to the need for a large volume of the highly reactive Ba-Cu-O molten liquid precursor and its reactions with the substrate.

Later on, the hybrid liquid phase epitaxy (HLPE) method was developed and this had the advantage of being able to use standard thin film growth equipment, rather than a large crucible of liquid. In it a thin liquid layer ( $\sim 1 \mu\text{m}$ ) is initially deposited on the substrate [9] [10], after which vapour species are delivered to the liquid surface, supersaturating it, and forcing REBCO to crystallize out onto the substrate surface. The REBCO formation rate is high (as in LPE) owing to the much enhanced diffusion rates of RE species in liquid compared to surface diffusion rates on a substrate surface. Growth rates of 500 nm/min and self-field  $J_c$ 's over 1 MA/cm<sup>2</sup> in 3  $\mu\text{m}$  thick films at 77 K [11] are achievable. However, the process has the disadvantage of being two-step, with the liquid layer needing to be deposited before the REBCO growth step. Also, the process has intrinsically lower supersaturation than other standard vapour processes, requiring careful control of the processing to produce high performance films. A third liquid process, with industrial success, is the process developed by SuNAM [12] which is based on ex-situ liquid processing. It has an extremely fast conversion rate (over 100 nm/s) [13] and involves the deposition of an amorphous non-stoichiometric RE-Ba-Cu-O film, followed by conversion, ex-situ, to REBCO via a liquid after increasing the temperature and  $pO_2$  sequentially [12]. The process gives very high  $J_c$  (3.2 MA/cm<sup>2</sup>) conductors at 77 K in self-field [13] [14].

This work is aimed at applications where high critical currents ( $>\sim 1000 \text{ A}$ ) can be achieved in fields above 5 T which means operating at  $\sim 30 \text{ K}$  or below. It is also aimed at lower cost conductor. This necessitates creating films at fast growth rates with very strong pinning engineered into them.

To achieve fast growth rates, the presence of liquids during growth is highly beneficial. To achieve strong pinning in the field range of interest, a mixed pinning morphology is needed, i.e. extended 1D (columnar) artificial pinning centres (APCs), plus 0D-like (point defects) [15].

To achieve the aforementioned goals of high performance at fast growth rates, we have developed a new process termed liquid assisted processing (LAP) in PLD. LAP is a simple *in-situ* process in which small ( $\sim 6 \text{ vol.}\%$ ) liquid fractions are incorporated in the films during growth, through the use of a non-stoichiometric target. The method is expected to be adaptable to a wide range of physical or chemical vapour deposition processes.

We aim to create a mixed pinning landscape of both columnar APCs and isotropic low dimensional point pinning defects. To create columnar APCs in the film we need to be selective about which APCs will form in the presence of the liquid. This is discussed further in the experimental section.

As far as point pinning defects goes, we hypothesize that they will be created by using mixed rare-earths REBCO films, i.e. using at least two REs of different atomic sizes to create  $\text{RE}_{1-x}\text{RE}_x\text{BCO}$  films [3]. The difference in the size of the RE ions (ion size variance) [16] leads to localised regions of strain within the lattice which can potentially act as pinning sites [16] [17]. Additionally, for rare-earth ions of a similar size to the  $\text{Ba}^{2+}$  ion, Ba-RE cross substitution occurs creating further point defects [18] [19].  $x$  needs to be small in  $\text{RE}_{1-x}\text{RE}_x\text{BCO}$  so that the growth temperature can be optimised for RE1. If  $x$  is large then the growth temperature would not be optimised for either RE1 or RE2 and this would lead to poor overall crystallinity and likely irregular buckling of the CuO planes, both being detrimental to superconductivity.

Samples with a mixed rare-earth component have been shown to have mildly improved performance at 77 K [20] [21] [22] [23]. However, it is at lower temperatures that such point defects are expected to be most beneficial, with previous studies predicting that they will become the major contribution to the vortex pinning force at low temperatures [24].

## Experimental

PLD targets were made from single phase powders of  $Y_2O_3$ ,  $Ba(NO_3)_2$ ,  $CuO$  and, where needed, powders of  $Sm_2O_3$  and  $Yb_2O_3$ . All powders were weighed to the appropriate amounts, mixed by hand, ground, pressed and finally reacted at 850 °C in oxygen for 24 hours. The targets were then re-ground and re-sintered to ensure homogeneity and that a complete reaction occurred. Six different composition targets were made, as shown in Table 1.

For mixed RE targets, the at. % of Y was always 80 % so that the growth temperature could be kept the same for all films. To balance the 80 at. % Y, and hence ensure stoichiometry, we used 20% additions of the RE additives. We used rare-earths smaller ( $Yb^{3+}$ ), larger ( $Sm^{3+}$ ) or a combination of smaller and larger ( $Yb^{3+}$ ,  $Sm^{3+}$ ) than the matrix rare-earth ( $Y^{3+}$ ).

Two of the LAP films had 5 mol. %  $Ba_2YNbO_6$  (BYNO) APCs added to them (Table 1). One film was pure YBO and the other a mixed RE film. BYNO was chosen as previous works showed that BYNO additions produce strong *c* axis pinning (up to twice the  $J_c$  for  $H \parallel c$  as compared to pure YBCO films [25]), even at relatively high growth rates ( $> 1$  nm/s). Hence, BYNO can self-assemble into nanocolumns at high growth rates where other APCs cannot [25] [26]. Since LAP is a fast process, it is important to use an APC which will assemble into nanocolumns (rather than nanoparticles) at fast growth rates.

The position of the (Y+RE):Ba:Cu ratio used in all the targets is shown on the phase diagram of Figure 1 as a red dot. We show only Y rather than Y+RE on the diagram for simplicity. The target compositions are also listed in Table 1 but all have a (Y+RE):Ba:Cu ratio of 1:1.7:2.7, i.e. a target rich in (Y+RE) and Cu compared to YBCO (as can be more easily seen if the composition is normalised to  $Ba = 2$ , namely 1.18 : 2.00 : 3.18). This ratio was found to be the optimal based on our exploration of cation ratios near to the 1:2:3 ratio, particularly ones which had more Cu or more Y. The 1:1.7:2.7 ratio was found to give the strongest (001) peaks and highest  $T_c$  and  $J_c$ (77 K, self-field) values.

The phase diagram for  $Y_2O_3$ - BaO-CuO is shown in Figure 1 predicts above the peritectic temperature under reducing oxidation conditions (i.e. above ~800 °C and  $pO_2 < 0.1$  Torr). Hence, the 1:1.7:2.7 composition will form a mixture of (Y+RE)BCO, liquid and  $Y_2BaCuO_5$  (see blue triangle). However, owing to kinetic factors and epitaxial stabilisation by the forming *c*-aligned (Y+RE)BCO, (Y+RE) $_2O_3$  forms in the films instead of (Y+RE) $_2BaCuO_5$  during LAP growth [27]. Hence, the phases which form are those at the vertices of the ‘kinetic’ tie triangle (shown in red in Figure 1), i.e. 1:2:3 + liquid +  $Y_2O_3$  (we ignore the (Y+RE) $_2O_3$  mixed composition, for simplicity here). The position of the liquid phase boundary is not precisely known under the conditions found during growth and is estimated in Figure 1. However an approximation of the phase ratios, assuming the positions shown in the ‘kinetic’ tie triangle of Figure 1, gives the mol.% and approximate vol.% (assuming equal volume per atom) of YBCO,  $Y_2O_3$  and liquid during the growth to be 88 mol.%, 10 mol.%, 2 mol.%, or 91 vol.%, 3 vol.%, 6 vol.%, respectively.

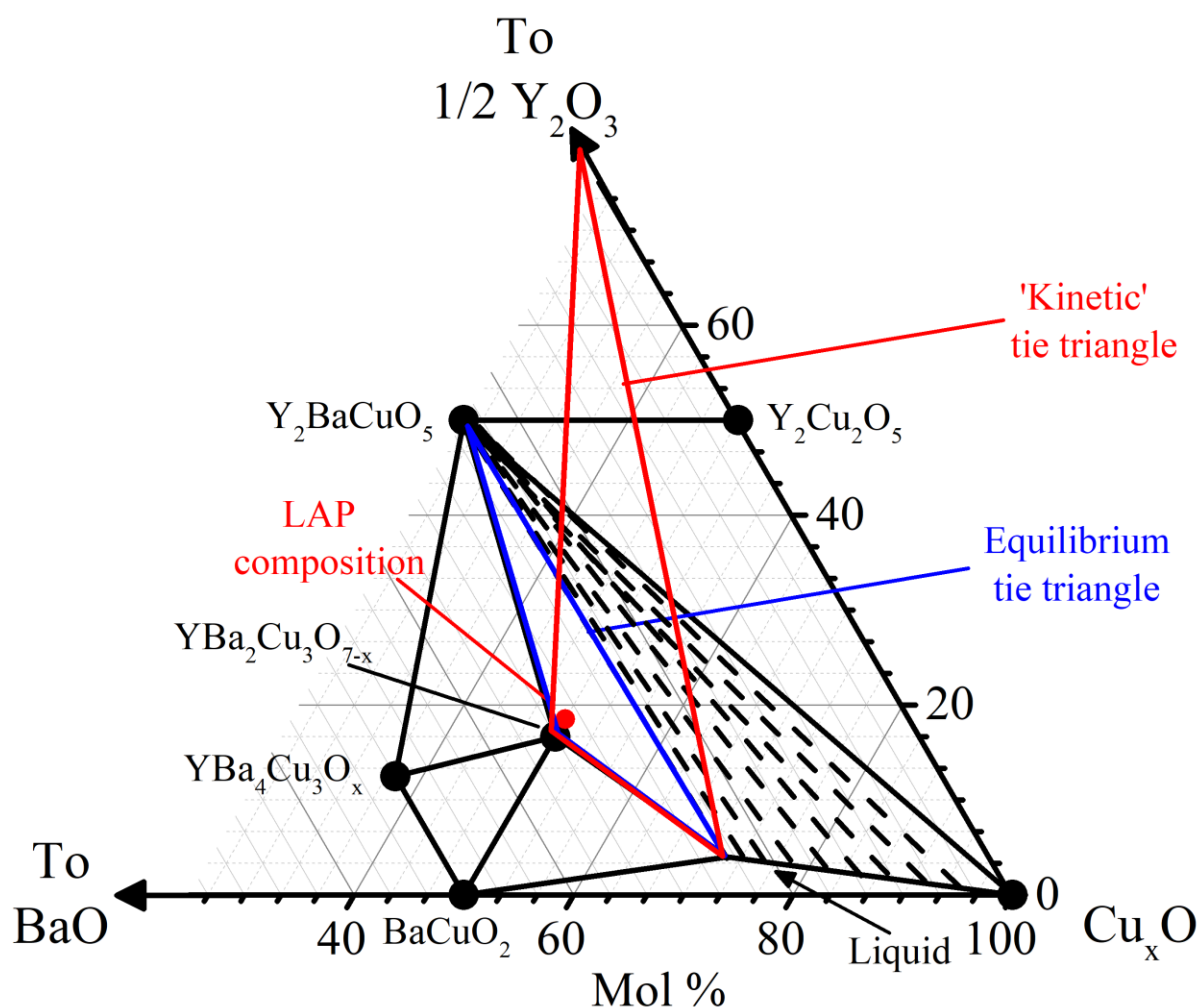


**Figure 1** Ternary phase diagram of Y-Ba-Cu under a constant low  $pO_2$  ( $<0.1$  Torr.) and temperature of 800 °C. Adapted from [28] [29]. Although at equilibrium the phases expected to form are given by the tie triangle around the composition of interest (blue), kinetic and epitaxial growth effects modify this, leading instead to the formation of YBCO, liquid and  $Y_2O_3$  (shown by the red ‘kinetic’ tie triangle). In this study, some of our compositions have 20% of other REs substituted for Y, but the phase diagram is assumed to be qualitatively the same as for pure Y.

Differential scanning calorimetry (DSC) measurements were conducted using a TA Instruments Q600 SDT on ~ 10 mg of ground sintered target material. Heating rates of 15 °/min were used in a nitrogen atmosphere. The eutectic and peritectic temperatures,  $T_E$ , and  $T_P$ , respectively, were both determined from the DSC measurements (shown in **Supplementary Note 1**). This data guided our understanding of the optimum growth temperature to use for the films. The minimum requirement for the LAP process to work is for there to be a liquid present. This means operating marginally above  $T_E$ . We determined that 820°C enabled this for all compositions. We note, however, that since the  $T_E$  and  $T_P$  values varied by more than 25°C across compositions, there would certainly be scope for further individual growth temperature optimisation for each specific composition.

All films are grown using pulsed laser deposition (PLD) at 820°C. A Lambda Physik KrF excimer laser was used ( $\lambda = 248$  nm, fluence  $\sim 2$  J/cm<sup>2</sup>,  $\sim 0.15$  J/pulse) on single crystal (100) SrTiO<sub>3</sub> (STO) substrates. A laser pulse repetition rate of 50 Hz was used which created a growth rate of  $\sim 250$  nm/min. This growth rate is higher than standard YBCO PLD film growth by a factor of  $\sim 4$ -60 [26] [30]. The high growth rate is enabled by the presence of a liquid phase in the films during deposition. The growth  $pO_2$  of all the films was 200 mTorr  $pO_2$ , and after growth the films were oxygenated at 500 °C in 760 Torr  $pO_2$  for one hour. All films had thicknesses of 350 nm  $\pm$  20 nm. The deposition temperatures of the films were in the range 750 °C – 850 °C, with the temperature of the heater controlled using a conventional thermocouple-P.I.D. controller.

After growing over this range of temperatures, the optimum growth temperature was determined by finding the lowest value of full-width-half-maximum (FWHM) of the (005) X-ray peak, indicative of very high crystalline perfection and the highest  $T_c$  and  $J_c$  (77 K, self-field).

The transition temperature ( $T_c$ ) and the critical-current-density-field dependency ( $J_c(B)$ ) were measured using a conventional four-point probe method. The critical current density measurements used a 1  $\mu$ V cm<sup>-1</sup> criterion, the maximum Lorentz force configuration and were conducted on samples etched to have 25  $\mu$ m wide bridges. The bridges were patterned using a standard photolithographic method with silver electrical contact pads deposited to ensure high quality contact interfaces. After measurement the thicknesses of the films were determined via a Dektak stylus profilometer.

A Philips PW3020 diffractometer employing CuK $\alpha$  radiation was used to carry out structural analysis. X-ray diffraction in the Bragg-Brentano geometry and rocking curves of the (005) YBCO peak, (the highest intensity (001) peak), were carried out to study the phases developed in the films and their epitaxial quality. A FEI Nova NanoSEM was also used to create scanning electron microscope images to investigate the surface of the films. Cross-sectional transmission microscopy (TEM) was used to image the BYNO nanoinclusions in the YBCO matrix.

Composition no.	RE:Ba:Cu ratio	RE Composition (Y = 80% + other RE(s) = 20%)	Film Composition acronym	$T_c$ at optimum growth T $\pm 0.1$ K /K	$c$ at optimum growth T ( $\text{\AA}$ )	Lowest FWHM of (005) peak in $\theta$ -2 $\theta$	Rocking curve width of (005) peak	$J_c$ (50K, 5T) / MA.cm <sup>-2</sup>	$J_c$ (10K, 10T) / MA.cm <sup>-2</sup>
<b>50 Hz growth high rate (HR) – no LAP</b>									
1	1:2:3	Y	Y123	79.1	11.72	0.369	0.348	0.8	1.4
<b>50 Hz growth high rate (HR) + LAP</b>									
2	1:1.7:2.7	Y	Y123+liquid	91.2	11.72	0.318	0.405	1.7	4.5
3	1:1.7:2.7	Y, Yb	(Y,Yb)123 + liquid	86.9	11.67	0.472	0.594	0.8	3.8
4	1:1.7:2.7	Y, Sm	(Y,Sm)123 + liquid	85.2	11.74	0.523	0.587	0.9	4.7
5	1:1.7:2.7	Y, Yb, Sm	(Y,Yb,Sm)123 + liquid	88.4	11.71	0.427	0.542	1.5	4.3
<b>50 Hz growth high rate (HR) + LAP + BYNO</b>									
6	1:1.7:2.7	Y	Y123+liquid+BYNO	89.3	11.71	0.345	0.530	2.1	4.6
7	1:1.7:2.7	Y, Yb, Sm	(Y,Yb,Sm)123 + liquid + BYNO	86.6	11.71	0.384	0.519	2.0	7.7

**Table 1:** Details of compositions studied, liquid formation temperature, optimum film growth temperatures and  $J_c$  (50 K,5T) and (10 K 10 T). All films were grown at 50 Hz laser repetition rate. Note: The RE ion sizes are  $Y^{3+} = 1.02 \text{ \AA}$ ,  $Yb^{3+} = 0.98 \text{ \AA}$ ,  $Sm^{3+} = 1.09 \text{ \AA}$  [31].

## Results & Discussion

Table 1 above shows all the compositions studied and information on their structural features,  $T_c$ 's and  $J_c$ 's of the films at different  $H$  and  $T$ . As determined from the low FWHM of the (005)  $\theta/2\theta$  and  $\omega$  scans, the films were all highly aligned and had excellent crystallinity, much more so than the plain YBCO film grown at 50 Hz (denoted Y123). As shown in **Supplementary Note 2** (for sample #2 in Table 1), the highest  $T_c$  coincided with the lowest level of structural disorder (as determined from the lowest FWHM of the (005) peak) and lowest  $c$  parameter, both indicative of optimum crystalline perfection. This occurred at 820 °C, a temperature at which the film growth would be in the presence of liquid at a  $pO_2$  of 200 mTorr. This temperature is higher than typically used during REBCO PLD growth by more than 30 °C [32] [33], in order to ensure sufficient liquid is present.

We first consider the reference *stoichiometric* YBCO sample (Y123, sample #1). The film was grown with no liquid present and had a reduced  $T_c$  of 79.0 K. The lower  $T_c$  is unsurprising considering the structural disorder which is induced at such high growth rates [34]. The  $c$  parameter of the high rate film is 11.72 Å is high compared to the bulk value of 11.69 Å found in low-rate-grown YBCO films and is indicative of some cation disorder [31] [35].

For the RE-added films, the  $c$ -parameter trend follows the pattern expected from the size of the rare-earths, with the (Y,Yb)123+liquid (#3) film having the smallest  $c$  value (11.67 Å), the (Y,Sm)123+liquid film (#4) having the largest  $c$  value (11.74 Å) and the (Y,Yb,Sm)123+liquid film (#5) in between (11.71 Å). The  $T_c$ 's of all the mixed RE films with LAP are lower than pure YBCO with LAP. Of the mixed RE films, the highest  $T_c$  value is for the (Y,Yb,Sm)123+liquid film (88.4 K), i.e. it is higher than the (Y,Yb)123+liquid or (Y,Sm)123+liquid films by up to 3 K. This is likely because the average RE ionic radius in these films (i.e. average of large Sm, middle Y and small Yb) of 1.03 Å is close to the radius of pure Y at 1.02 Å [31], whereas it is either considerably higher or lower for the other compositions.

The  $T_c$ 's for films containing BYNO (i.e. samples #6 and #7, Table 1) were slightly lower (by 2 K) than the parent films which did not contain BYNO. This is common for REBCO films that include secondary phases and occurs due to the structural perturbation of the REBCO lattice by the APC [30] [36]. This is manifest as higher FWHM values in the (005) peak in the  $\theta$ - $2\theta$  and  $\omega$  scans, i.e. values of  $\sim 0.34^\circ$  and  $\sim 0.53^\circ$  (#6), respectively. On the other hand, there was only a marginal effect on the  $c$  parameter, which agrees with a previous study on BYNO doped YBCO [30]. Hence, while there is structural disruption (i.e. buckling of planes and tilting of grains), there is little or no induced cation disorder induced in the REBCO lattice.

Structural disruption in the mixed RE-123 films would be expected to give rise to higher FWHM values for the (005) peaks in the  $\theta$ - $2\theta$  and  $\omega$  scans. We indeed find this to be the case for all the mixed-RE films. The largest structural disorder, lowest  $T_c$  sample, (Y,Sm)123+liquid (#4) had the largest values of  $\theta$ - $2\theta$  FWHM value of all the films. Compared to the Y123+liquid film (#2), the FWHM was  $\sim 0.52^\circ$  *cf.*  $\sim 0.32^\circ$ . It also had the largest  $\omega$  scan FWHM value of all the films, i.e.  $\sim 0.59^\circ$  *cf.*  $\sim 0.40^\circ$ , compared to Y123+liquid sample (#2).

XRD  $\theta/2\theta$  scans of an optimised YBCO films made by the LAP process (i.e. Y123+liquid, sample #2) is shown in the top half of Fig. 2a. The mixed RE films showed very similar patterns in terms of sharp (00 $l$ ) peaks and similar second phase peaks. The bottom half of Fig. 2a also shows a film made by the LAP process, but now doped with BYNO (i.e. Y123+liquid+BYNO, sample #6). A clear (400) BYNO peak is observed, as seen in previous BYNO-doped YBCO films [25] [37] [38], indicating that

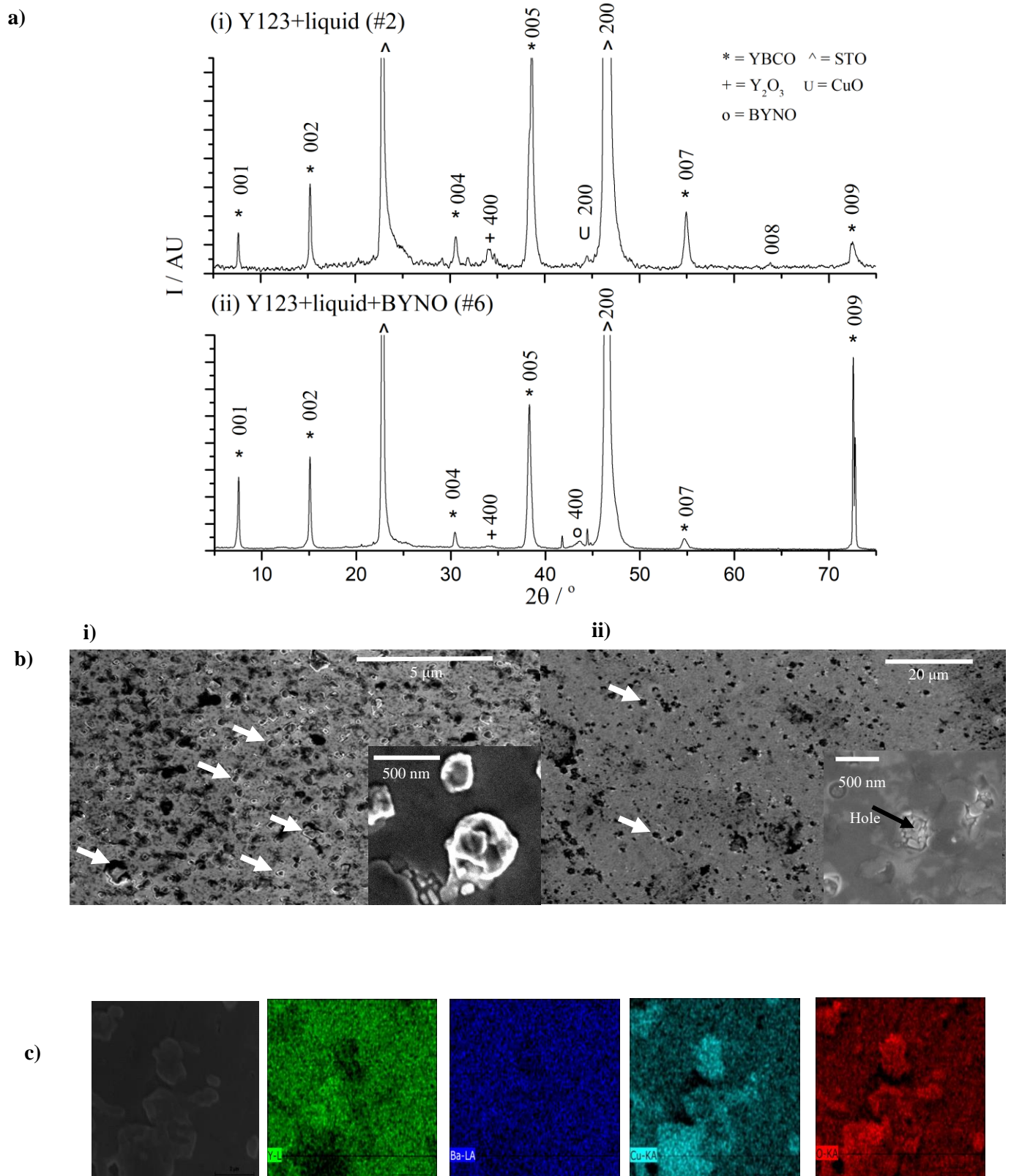


**Figure 2. Structural and microstructural features of films grown by the LAP process.** All films were grown at 820 °C and 50 Hz. **a)**  $\theta/2\theta$  traces for (i) film of undoped LAP film (Y123+liquid, # 2) and (ii) BYNO doped LAP film, (Y123+liquid+BYNO, # 6). The  $\theta/2\theta$  labels indicate: \* = (00l) YBCO peaks, + = 004 RE<sub>2</sub>O<sub>3</sub> peaks, U = (200) CuO peaks, o = (400) BYNO peaks, ^ = (00l) (substrate) STO peaks. **b)** SEM surfaces images of film # 2 showing surfaces features highlighted by arrows (i) round surface particles and (ii) holes **(c)** EDX mapping revealing the round particles are Cu-rich, indicative of solidified Cu-rich liquid. This liquid is apparent in the phase diagram of Figure 1.



*c*-axis oriented BYNO nanocolumns have formed. This was confirmed in cross-sectional TEM images of the films (discussed later). Other phases observed in the X-ray patterns for these films, and all other films grown by the LAP process, are  $Y_2O_3 + CuO$ .  $Y_2O_3 + CuO$  are phases commonly observed in liquid processed films [14].  $Y_2O_3$  forms due to the excess Y and because it is epitaxially stabilised when YBCO crystallises [28] and CuO forms from the liquid when the film cools after deposition [14].

There was evidence from SEM of the presence of a liquid phase in the LAP films. Figure 2b and 2c show example images for sample #2. We see a faceted, surface, secondary-phase particles (Fig. 2bi), as well as shallow holes surrounded by very smooth regions (Fig. 2bii). EDX maps (Fig. 2c) confirm the faceted surface particles are Cu-rich (indicative of CuO) and the shallow holes likely form due to contraction of the liquid when it solidifies upon cooling, both indicative of a surface formed from a crystallised liquid.

We now turn to critical current density ( $J_c$ ) measurements. Figure 3 shows  $J_c$  versus field,  $B$ ,  $\parallel c$  plots for fields up to 11 T at 70 K, 50 K, 30 K and 10 K. We include here all LAP films grown at 50 Hz (#2-#7). We also include the reference 50 Hz YBCO film grown without LAP (Y123, film #1).

First, we observe that the YBCO film grown with LAP at 50 Hz, i.e. film Y123+liquid (#2), has a considerably higher  $T_c$  and  $J_c$  (by over an order of magnitude at many fields and temperatures) than the stoichiometric YBCO film grown at the same rate but without LAP (#1). The faster diffusion rates available with LAP films would have allowed for a higher quality REBCO crystalline lattice to form, and hence to much less structural perturbation than in the stoichiometric YBCO film, leading to the much improved  $T_c$  and  $J_c$ . This is a significant result since it is proof that even if point-like disorder is induced by the high growth rates, as might be expected for very-fast-grown stoichiometric YBCO, this alone will not be effective for increasing  $J_c$ . Instead the disorder induced into REBCO (either by fast growth or by mixing REs) needs to be carefully engineered so that the REBCO lattice itself is not perturbed or disrupted to any large extent, in particular in terms of buckling of, or disconnecting the CuO planes.

Next, we observe in Fig. 3 that the  $J_c$ s of the mixed RE films are generally high, and more so with decreasing temperature compared to Y123 + liquid. The high  $J_c$  values for the mixed RE films are exemplified by the ‘50K, 5T’ and ‘10K, 10T’, values shown in Table 1. Hence, introducing liquids into the films enables intrinsic disorder from RE mixing to be effective for pinning even when fast growth rates are used. The benefits of using RE mixing to give high  $J_c$ s has not been reported before for high rate grown films. This is likely because in the absence of liquids the kinetics are insufficient to ‘heal’ more long range disorder which is induced from the highly dense atomic disorder associated with the RE1 and RE2 ion size differences in the  $RE_{1-x}RE_2_xBCO$ .

Looking at the 70 K data first, for samples where the lattice FWHM values are the same, then one would expect the BYNO-added APC films to have superior in-field  $J_c$  because of the positive APC pinning effect. In line with this reasoning, the best performing sample is indeed Y123+liquid+BYNO (#6). One might then expect the (Y,Yb,Sm)123+liquid+BYNO film (#7) to be the next in order. However, at this measurement temperature the  $T_c$  of the sample is important: if  $T_c$  is depressed much from 91 K, this will reduce the overall performance. Since the  $T_c$  of #7 is somewhat depressed by the RE mixing, to 86.6 K, the pure Y123+liquid film (#2) takes the second place slot, with #7 coming third. After this, since there are no further APC doped films, the trend in  $J_c$  then simply reflects the trend in  $T_c$ : i.e. (Y,Yb,Sm)123+liquid (#5), then (Y,Yb)123+liquid (#3), then (Y,Sm)123+liquid (#4)

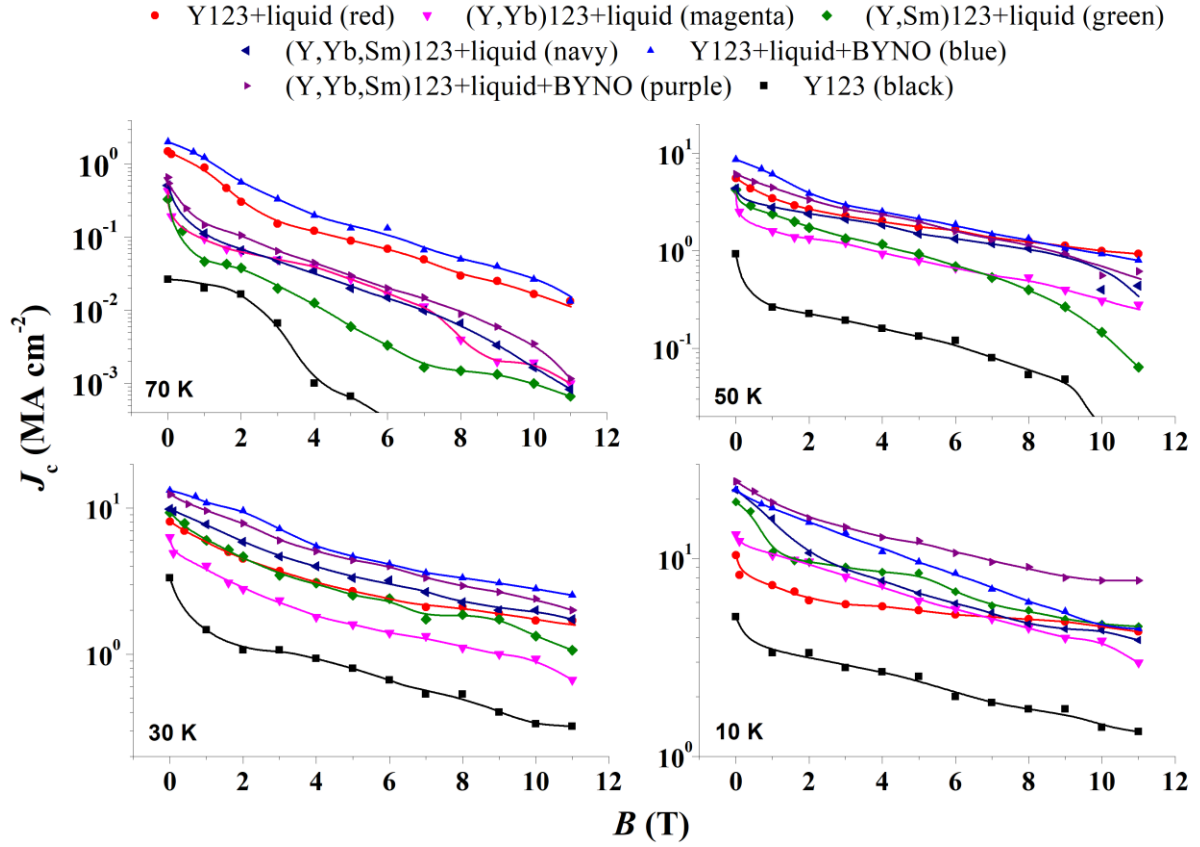


**Figure 3** Critical current density ( $J_c$ ). Data measured on films deposited at 820 °C and 50 Hz. Film # 1: Y123 (black); Film #2: Y123+liquid (red); film #3: (Y,Yb)123+liquid (magenta); film #4: (Y,Sm)123+liquid (green); film #5: (Y,Yb,Sm)123+liquid (navy); film #6: Y123+liquid+BYNO (blue); film #7: (Y,Yb,Sm)123+liquid+BYNO (purple). The lines between points are guides for the eye only. The plot shows at least two distinctive regimes present. However, at higher temperatures (70 K and 50 K) three different regions are seen. The first one goes up to  $B_0$ , here between 1 T and 2 T, which is typical for films containing nanocolumns. The second regime is seen as dominated by an exponential decay with an  $\alpha$  exponent given by  $J_c \sim B^{-\alpha}$ . The third regime shows rapid decay of  $J_c$  as the matching field and irreversibility line are approached.

and then Y123 (#1). We note that any point pinning centres from the RE mixing are easily thermally depinned at this temperature [24] and so produce no benefit.

At 50 K, the (Y,Yb,Sm)123+liquid+BYNO film (#7) shows a relatively improved performance compared to the 70 K data and now is close to the Y123+liquid+BYNO (#6) sample despite having a lower  $T_c$  (86.6 K *cf.* 89.3 K). This reveals the strong pinning in this sample from RE mixing effects, over and above the BYNO APC pinning, and the lesser importance of  $T_c$ . The (Y,Yb,Sm)123+liquid film (#5) also shows a relatively improved performance *cf.* to at 70 K, despite the poorer crystallinity as revealed by the x-ray data, as discussed earlier. Finally, the (Y,Sm)123+liquid (#4) film rises relative to its respective place at 70 K, although not by as much as #7 and #5. This is likely because both  $T_c$  (86.9 K) and crystallinity are, overall, the worst in sample #4 *cf.* all the other LAP samples, as shown in Table 1. The results indicate that the additional point disorder induced by the rare-earth mixing acts as effective pinning centres. These defects are likely to be nano-strain fields in the crystal

structure arising from the different sizes of the mixed REs [16]. As already noted, while mixed RE films grown in the absence of liquid have not, as far as known, been shown to give rise to effective point pins, this may be because of more long-range disruption of the REBCO lattice when there is no liquid to ‘heal’ the disruption.

At 30 K, the Y123+liquid+BYNO film (#6) continues to perform the best of the samples, indicative of the strong influence of pinning by the nanocolumns. Effective nanocolumnar pinning at 30 K is agreement with what has been found already for standard REBCO films with APCs [39]. The films with mixed REs show similarly good performance at 30 K *cf.* 50 K. Hence, the (Y,Yb,Sm)123+liquid+BYNO (#7) is nearly as good as the Y123+liquid+BYNO film (#6). However, the pure Y123+liquid film (#2) falls further behind *cf.* 50 K and 70 K, because it has no APC or point like pinning centres engineered into it. The (Y,Yb,Sm)123+liquid (#5) is the next best sample, similar to at 50 K. Then, interestingly, compared to at the higher temperatures, (Y,Sm)123+liquid (#4) swaps its order with (Y,Yb)123+liquid (#3). This is because the effect of the lower  $T_c$  of #4 is lessened (#4 has the poorest  $T_c$ , 86.9 K, and poorest crystallinity of all the samples). Instead, its point pins from the RE mixing begin to be more effective, and there are more of them in #4 than #3. Overall, the 30 K data shows that *both* the APCs and RE mixing-related point pinning both play a stronger role in determining  $J_c(B)$  and that at this lower temperature the effect of a reduced  $T_c$  is lessened compared to the higher temperature measurements.

At 10 K, the optimum performing film is (Y,Yb,Sm)123+liquid+BYNO (#7). It now outperforms Y123+liquid+BYNO (#6) which was optimum at 30 K. This data further proves that at low temperatures both APC and mixed-RE point like pinning both play strong roles. It also shows that at the lowest temperatures the importance of point pins arising from mixing of REs increases significantly. These point pins provide a weak 0D-like pinning landscape which very effectively supplements the stronger pinning defects arising from the APC columns, leading to very high pinning forces at 10 K, similar to some of the best in the literature, despite the x4-60 faster growth rates.

In terms of the performance of these conductors compared to other liquid processed films grown at similar rates, e.g. an ex-situ film made by SuNAM Ltd, the  $J_c$  for films in this study are up to three times higher at 3 T, and six times higher at 5 T [13]. Also, compared to standard stoichiometric YBCO films with BaZrO<sub>3</sub> and Ba<sub>2</sub>Y(Nb,Ta)O<sub>6</sub> pinning additives, the *in-situ* LAP films show similar performance over a range of fields from 70 K to 30 K and they outperform these standard APC films at 10 K (by up to a factor of 2), despite being grown 4-60 times faster [26].

While it is not possible to image the point-like defects arising from the RE mixing by TEM, it is still important to confirm the nature of the BYNO APC additions to the films which, so far, we’ve presumed to be columnar owing to the improved  $J_c$  vs  $B \parallel c$ . In Figure 4, we show an example of a Y123+liquid+BYNO LAP film (the same film process as #6). We indeed observe the presence of  $c$ -axis correlated BYNO nanocolumns. Hence BYNO nanocolumns have time to assemble despite the very fast growth rates which have typically prevent APCs assembling into well-formed columns [15]. The columns are ~ 5 nm in diameter, spacings ~ 20-30 nm, with ~ 40 nm long segments stacked on top of one another (Figure 4a). The YBCO lattice between the columns remains highly aligned between the dense, fine columns (as shown in the higher resolution image of Figure 4b). Although the columns are shorter than the through-thickness columns reported under standard growth conditions for some APCs [36] [40], this is likely not because of a kinetic limitation, but rather because of strain and thermodynamic factors related to BYNO which has a large lattice mismatch with YBCO [15].

The BYNO columns would be expected to act as very strong extended 1D pinning centres for  $B \parallel c$ , explaining the observed behaviour seen in the  $J_c$  measurements. Also, we note that the density of columns is high enough that there are likely to be ‘secondary-effect’ point like defects associated with

the columns as they disrupt the REBCO matrix around themselves [15]. This has been effectively seen for MOCVD conductors with 15 at.% BaZrO<sub>3</sub> additions [41].

Finally, we note that while the LAP method demonstrated here for PLD growth could also easily be adapted to other physical or chemical vapour deposition methods to achieve very high-performance conductors at an order of magnitude higher rate, and hence at lower cost.

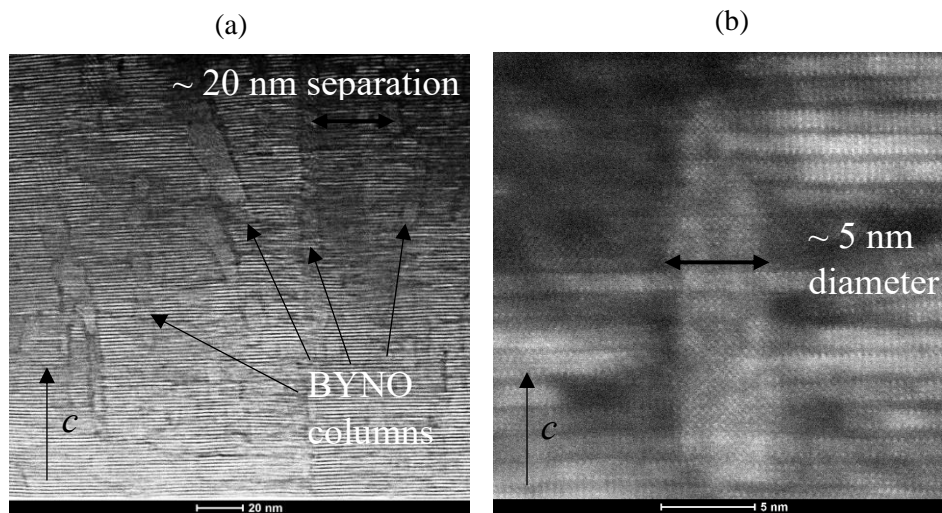


**Figure 4** Cross sectional TEM images of films showing (a) BYNO columns aligned parallel to  $c$ , spaced  $\sim 20$  nm apart with (b) a diameter of  $\sim 5$  nm.

## Conclusions

Fast growth of REBCO coated conductors with strong pinning is essential to reduce the cost of superconducting applications. This paper presents the results of a new *in-situ* liquid assisting processing (LAP) method that utilises PLD deposition. The method allows for very fast growth rates (up to 250 nm/s), i.e. more than an order of magnitude faster than standard films. The method enables extended Ba<sub>2</sub>YNbO<sub>6</sub> nanocolumnar artificial pinning centres (APCs) to form despite the very fast growth rates, as well as point-like defect pinning centres to be created by having mixed rare-earths in the films. The mixed pinning, mixed RE + BYNO LAP films were shown to be very effective for pinning at 10 K, 30 K and 50 K. Compared to standard YBCO films grown by PLD with different APC pinning additives, despite the much faster growth rates, the LAP films showed similar  $J_c$ s over a range of fields from 70 K to 30 K, while at 10 K they outperformed the standard films by up to a factor of  $\sim x 2$ . An increasing influence of point-like pinning from RE mixing in the films at lower temperatures was demonstrated. The LAP method holds much promise for lowering coated conductor cost compared to growth using standard *in-situ* vapour growth methods, simply by modifying the composition of the target material.

## References

- [1] Obradors X Puig T, Coated conductors for power applications: materials challenges, *Supercond Sci Technol*, **27**, 4, 2014  
<https://doi.org/10.1088/0953-2048/27/4/044003>
- [2] Fietz W et al, Prospects of High Temperature Superconductors for fusion magnets and power applications, *Fusion Eng Des*, **88**, 6, pp. 40, 2013

- <https://doi.org/10.1016/j.fusengdes.2013.03.059>
- [3] S. R. Foltyn et al, Materials science challenges for high-temperature superconducting wire, *Nat Mater*, **6**, pp. 631-642, 2007  
<https://doi.org/10.1038/nmat1989>
- [4] Qi X., MacManus-Driscoll J.L., Liquid phase epitaxy processing for high temperature superconductor tapes, *Curr. Opin. Solid State Mater Sci*, **5**, pp. 291–300, 2001  
[https://doi.org/10.1016/S1359-0286\(00\)00040-1](https://doi.org/10.1016/S1359-0286(00)00040-1)
- [5] Kursumovic A et al., Study of the rate-limiting processes in liquid-phase epitaxy of thick YBaCuO films, *J Cryst Growth*, **218**, 1, pp 45-56, 2000  
[https://doi.org/10.1016/S0022-0248\(00\)00519-4](https://doi.org/10.1016/S0022-0248(00)00519-4)
- [6] MacManus-Driscoll J. L., High  $I_c$  in YBCO Films Grown at Very High Rates by Liquid Mediated Growth., *IEEE Trans Appl Supercond*, 19, 3, 2009  
<http://dx.doi.org/10.1109/TASC.2009.2018850>
- [7] Kuphal E., Liquid Phase Epitaxy, *Appl Phys A*, **52**, pp. 380-409, 1991  
<https://doi.org/10.1007/BF00323650>
- [8] Hirabayashi I., High  $J_c$  YBCO thick films prepared by LPE method, *IEEE Trans Appl Supercond*, **5**, 2, 1995  
<https://doi.org/10.1109/77.402982>
- [9] Kursumovic A. et al., High critical current densities in YBa<sub>2</sub>Cu<sub>3</sub>O<sub>7-x</sub> films grown at high rates by hybrid liquid phase epitaxy, *Appl Phys Lett*, **87**, 25, 2005  
<https://aip.scitation.org/doi/10.1063/1.2149975>
- [10] Kursumovic A., Hybrid liquid phase epitaxy processes for YBa<sub>2</sub>Cu<sub>3</sub>O<sub>7</sub> film growth, *Supercond Sci Technol*, **17**, 10, 2004  
<https://doi.org/10.1088/0953-2048/17/10/024>
- [11] Maiorov B. et al., Vortex pinning landscape in YBa<sub>2</sub>Cu<sub>3</sub>O<sub>7</sub> films grown by hybrid liquid phase epitaxy, *Supercond Sci Technol*, **20**, 9, 2007  
<https://doi.org/10.1088/0953-2048/20/9/S17>
- [12] J. H. Lee et al., RCE-DR, a novel process for coated conductor fabrication with high performance, J. H. Lee et al., *Supercond Sci Technol*, **27**, 4, 2014  
<http://dx.doi.org/10.1088/0953-2048/27/4/044018>
- [13] Lee J. et al., Enhanced Pinning Properties of GdBa<sub>2</sub>Cu<sub>3</sub>O<sub>7-δ</sub> Coated Conductors via a Post-Annealing Process, *IEEE Trans Appl Supercond*, **26**, 3, 2016  
<http://dx.doi.org/10.1109/TASC.2016.2533629>
- [14] MacManus-Driscoll J. L. et al., Strong pinning in very fast grown reactive co-evaporated GdBa<sub>2</sub>Cu<sub>3</sub>O<sub>7</sub> coated conductors, *APL Mater*, **2**, 8, 2014  
<https://doi.org/10.1063/1.4893339>
- [15] Feighan J. et al., Materials design for artificial pinning centres in superconductor PLD coated conductors, *Supercond Sci Technol*, **30**, 12, 2017  
<https://doi.org/10.1088/1361-6668/aa90d1>
- [16] Rodriguez-Martinez L. M. et al., Cation disorder and size effects in magnetoresistive manganese oxide perovskites, *Phys Rev B: Condens Matter*, **54**, 22, 1996  
<https://doi.org/10.1103/PhysRevB.54.R15622>
- [17] Radhika Devi A. et al., Enhanced critical current density due to flux pinning from lattice defects in pulsed laser ablated Y<sub>1-x</sub>Dy<sub>x</sub>Ba<sub>2</sub>Cu<sub>3</sub>O<sub>7-δ</sub> thin films, *Supercond Sci Technol*, **13**, 7, 2000  
<https://doi.org/10.1088/0953-2048/13/7/305>
- [18] Kwon C. et al., Fabrication and characterization of (rare-earth)-barium-copper-oxide (RE<sub>123</sub> with RE=Y, Er, and Sm) films, *IEEE Trans Appl Supercond*, **9**, 2, 1999  
<https://doi.org/10.1109/77.784696>
- [19] Jia Q. X. et al., Comparative study of REBa<sub>2</sub>Cu<sub>3</sub>O<sub>7</sub> films for coated conductors, *IEEE Trans Appl Supercond*, **15**, 2, 2005  
<https://doi.org/10.1109/TASC.2005.847797>

- [20] MacManus-Driscoll J. L. et al., Systematic enhancement of in-field critical current density with rare-earth ion size variance in superconducting rare-earth barium cuprate films, *Appl Phys Lett*, **84**, 26, 2004  
<https://doi.org/10.1063/1.1766394>
- [21] MacManus-Driscoll J.D., Guidelines for optimizing random and correlated pinning in rare-earth-based superconducting films, *Supercond Sci Technol*, **19**, 3, 2006  
<https://doi.org/10.1088/0953-2048/19/3/008>
- [22] Wang P. F. et al., Effects of Sm-doping on Structures and Properties of YBCO Coated Conductors Fabricated by TFA-MOD Process, *J Supercond Nov Magn*, **25**, pp 261-266, 2012  
<https://doi.org/10.1007/s10948-011-1294-2>
- [23] Jha A. K., Matsumoto K., Superconductive REBCO Thin Films and Their Nanocomposites: The Role of Rare-Earth Oxides in Promoting Sustainable Energy, *Front Phys*, **7**, pp 82, 2019  
<https://doi.org/10.3389/fphy.2019.00082>
- [24] Puig T., Vortex pinning in chemical solution nanostructured YBCO films, *Supercond Sci Technol*, **21**, 3, 2008  
<https://doi.org/10.1088/0953-2048/21/3/034008>
- [25] Ercolano G. et al., Strong correlated pinning at high growth rates in YBa<sub>2</sub>Cu<sub>3</sub>O<sub>7-x</sub> thin films with Ba<sub>2</sub>YNbO<sub>6</sub> additions, *APL Mater*, **116**, 3, 2014  
<https://doi.org/10.1063/1.4890459>
- [26] Celentano G. et al., YBa<sub>2</sub>Cu<sub>3</sub>O<sub>7-x</sub> films with Ba<sub>2</sub>Y(Nb,Ta)O<sub>6</sub> nanoinclusions for high-field applications, *Supercond Sci Technol*, **33**, 4, 2020  
<https://doi.org/10.1088/1361-6668/ab6ee5>
- [27] Ohnishi T. et al., High Rate in situ YBa<sub>2</sub>Cu<sub>3</sub>O<sub>7</sub> Film Growth Assisted by Liquid Phase, *J Mater Sci*, **19**, 4, 2004  
<https://doi.org/10.1557/JMR.2004.0127>
- [28] Poole C., *Handbook of superconductivity*, Academic Press, London, 2000
- [29] Macmanus-Driscoll J.L., Materials chemistry and thermodynamics of REBa<sub>2</sub>Cu<sub>3</sub>O<sub>7-x</sub>, *Adv Mater*, **9**, 6, pp. 457-473 2004
- [30] Ercolano G. et al., Enhanced flux pinning in YBa<sub>2</sub>Cu<sub>3</sub>O<sub>7-δ</sub> thin films using Nb-based double perovskite additions, *Supercond Sci Technol*, **23**, 2, 2010  
<https://doi.org/10.1088/0953-2048/23/2/022003>
- [31] MacManus-Driscoll J. L., Studies of structural disorder in ReBa<sub>2</sub>Cu<sub>3</sub>O<sub>7-x</sub> thin films (Re=rare earth) as a function of rare-earth ionic radius and film deposition conditions, *Physica C*, **232**, 3, pp.288-308, 1994  
[https://doi.org/10.1016/0921-4534\(94\)90789-7](https://doi.org/10.1016/0921-4534(94)90789-7)
- [32] Greer J. A., High quality YBCO films grown over large areas by pulsed laser deposition, *J Vac Sci Technol*, **10**, 4, 1992  
<https://doi.org/10.1116/1.577753>
- [33] Gupta A. et al., Defect formation caused by a transient decrease in the ambient oxygen concentration during growth of YBa<sub>2</sub>Cu<sub>3</sub>O<sub>7-δ</sub> films, *APL Mater*, **57**, 22, 1990  
<https://doi.org/10.1063/1.104175>
- [34] Suh J. D., Sung G. Y., Crystal orientation control of YBa<sub>2</sub>Cu<sub>3</sub>O<sub>7-x</sub> thin films prepared by pulsed laser deposition, *Physica C*, **282**, 2, pp 579-580, 1997  
[https://doi.org/10.1016/S0921-4534\(97\)00381-X](https://doi.org/10.1016/S0921-4534(97)00381-X)
- [35] Gibson G. et al., A Raman measurement of cation disorder in YBa<sub>2</sub>Cu<sub>3</sub>O<sub>7-x</sub> thin films, *Physica C*, **333**, 3, pp 139-145 ,2000  
[https://doi.org/10.1016/S0921-4534\(00\)00093-9](https://doi.org/10.1016/S0921-4534(00)00093-9)
- [36] Harrington S. A. et al., Self-assembled, rare earth tantalate pyrochlore nanoparticles for superior flux pinning in YBa<sub>2</sub>Cu<sub>3</sub>O<sub>7-δ</sub> films, *Supercond Sci Technol*, **22**, 2, 2008  
<https://doi.org/10.1088/0953-2048/22/2/022001>

- [37] Wee S. et al., Formation of Self-Assembled, Double-Perovskite, Ba<sub>2</sub>YNbO<sub>6</sub> Nanocolumns and Their Contribution to Flux-Pinning and J<sub>c</sub> in Nb-Doped YBa<sub>2</sub>Cu<sub>3</sub>O<sub>7</sub> Films, *Appl Phys Express* **3**, 023101, 2010  
<https://doi.org/10.1143/APEX.3.023101>
- [38] Opherden L. et al., Large pinning forces and matching effects in YBa<sub>2</sub>Cu<sub>3</sub>O<sub>7-δ</sub> thin films with Ba<sub>2</sub>Y(Nb/Ta)O<sub>6</sub> nano-precipitates, *Sci Rep*, **6**, 21188, 2016  
<https://doi.org/10.1038/srep21188>
- [39] Xu A. et al., Strongly enhanced vortex pinning from 4 to 77 K in magnetic fields up to 31 T in 15 mol.% Zr-added (Gd, Y)-Ba-Cu-O superconducting tapes, *APL Mater*, **2**, 4, 2014  
<https://doi.org/10.1063/1.4872060>
- [40] Zhao R. et al., Precise Tuning of (YBa<sub>2</sub>Cu<sub>3</sub>O<sub>7-δ</sub>)<sub>1-x</sub>:(BaZrO<sub>3</sub>)<sub>x</sub> Thin Film Nanocomposite Structures, *Adv Funct Mater*, **24**, 33, 2014  
<https://doi.org/10.1002/adfm.201304302>
- [41] Galstyan E. et al., Correlation Between Microstructure and In-Field Performance of Zr-Added REBCO Coated Conductors Made by Advanced MOCVD, *IEEE Trans Appl Supercond*, **29**, 5, 2019  
<https://doi.org/10.1109/TASC.2019.2894276>

## SUPPLEMENTARY NOTE 1:

### Determining the relative melting points of the compositions used in this study

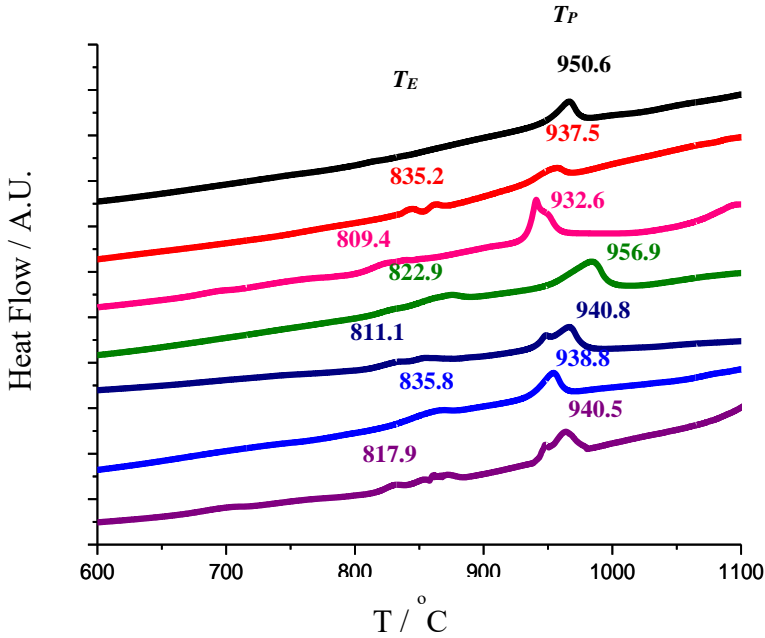


**Figure S1** DSC scans (heating rate 20 °C/min, N<sub>2</sub> atm) from powders of the compositions studied here. Y-1:2:3 (black), Y-1:1.7:2.7 (red), Y, Yb-1:1.7:2.7 (magenta), Y, Y, Sm-1:1.7:2.7 (green), Y, Yb, Sm-1:1.7:2.7 (navy), Y-1:1.7:2.7 + 5 mol.% BYNO (blue), Y, Yb, Sm-1:1.7:2.7 + 5 mol.% BYNO (purple)

Composition	$T_E$ (°C) (N <sub>2</sub> )	$T_P$ (°C) (N <sub>2</sub> )
Y-1:2:3	-	950.6
Y-1:1.7:2.7	835.2	937.5
Y, Yb-1:1.7:2.7	809.4	932.6
Y, Sm-1:1.7:2.7	822.9	956.9
Y, Yb, Sm-1:1.7:2.7	811.1	940.8
Y-1:1.7:2.7 + 5 mol.% BYNO	835.8	938.8
Y, Yb, Sm-1:1.7:2.7 + 5 mol.% BYNO	817.9	940.5

**Table S1** Eutectic and peritectic temperatures ( $T_E$  and  $T_P$ , respectively), measured by DSC under N<sub>2</sub> for the compositions used in this study (Fig. S1).

The temperatures for the onset of liquid formation ( $T_E$  the eutectic temperature and  $T_P$  the peritectic temperature) in a nitrogen atmosphere for the different compositions determined by differential scanning calorimetry (DSC) (**Figure S1**), are shown in **Table S1**. It is noted that, due to the nitrogen rich atmosphere,  $T_P$  is reduced by ~ 50 °C compared to air [S1][S2]. Additionally, we can see that melting peaks in the doped samples are at lower temperatures relative to YBCO.

The pure Y123 film, (composition Y-1:2:3) shows only  $T_P$  as the composition is stoichiometric. On the other hand, liquid assisted films show a  $T_E$  melting peak at a temperature lower than  $T_P$ , between 809.4-835.2 °C, consistent with the Ba<sub>2</sub>Cu<sub>3</sub>O<sub>y</sub> liquid phase melting temperature at low  $pO_2$  [S3].  $T_P$  is also higher for the Y, Sm -1:1.7:2.7 composition, at 956.9 °C, compared to the Y -1:1.7:2.7 composition, at 937.5 °C, which is expected because of the higher melting temperature of Sm-123, namely 1060 °C, than YBCO, 1005 °C [S4]. Likewise, the  $T_P$  for Y, Yb -1:1.7:2.7 was 932.6 °C, which is lower than for YBCO, again expected due to the lower  $T_P$  of Yb-123 cf Y-123 [S5]. The triple RE composition containing all 3 REs (Y, Yb, Sm -1:1.7:2.7) showed double/broader peaks, and the  $T_E$  and  $T_P$  temperatures determined from these peaks were 811.1 °C and 940.8 °C, which are closer to the Yb-containing sample, indicative of the presence of phase separation and the formation of two liquids. Furthermore, compositions doped with BYNO had similar  $T_P$  and  $T_E$  to the compositions



without BYNO. Having only a small change in melting temperatures on adding BYNO is expected as BYNO is not expected to interact with the Y123 system [S6].

We note that the  $pO_2$  during the DSC measurements is higher than that found in the deposition chamber during film growth. Furthermore, film growth is not at equilibrium and so even if the  $pO_2$  were the same in the DSC scan and deposition chamber the exact melting temperatures may not be replicated. The DSC data, therefore, acts as a guide to *relative* melting onset temperatures between the different films.

## Supplementary note 2:

Influence of growth temperature film composition Y= 1:1.7:2.7 deposited at high rate (50 Hz), sample #2 in Table 1.

Growth Temp. ( °C)	$T_c$ (K)	$c$ (Å) $\pm 0.001\text{Å}$	FMHM of (005) peak in $\theta$ -2 $\theta$ scan (°)	FHWM of (005) peak in rocking curve (°)
750	84.0	11.724	0.522	0.578
780	86.5	11.726	0.436	0.512
790	88.7	11.726	0.412	0.497
800	89.0	11.720	0.392	0.470
810	89.7	11.718	0.355	0.472
820	91.2	11.716	0.318	0.405
830	90.3	11.714	0.346	0.431
850	88.6	11.713	0.255	0.510

**Table S2** Growth temperature,  $T_c$ ,  $c$  parameter, and Full Width at Half Maximum (FWHM) of (005) peaks in x-ray  $\theta$ -2 $\theta$  and  $\omega$  curves for film Y123+liquid, composition #2 of Table 1.

For film Y, of composition Y=1:1.7:2.7 (sample 2, Table 1), deposited at 50 Hz, the highest  $T_c$  (91.2 K) was measured on films grown at 820 °C. This growth temperature is ~15 °C below the  $T_E$  for this composition, as shown in Table S1. However, the  $pO_2$  of the growth atmosphere is lower and so melting here is very likely. A growth temperature of 820 °C gives not only the highest  $T_c$  but also the minimum (005)  $\theta/2\theta$  peak FWHM, minimum (005) FWHM  $\omega$ -scan, and lowest  $c$  (which appears to plateau at 820 °C and above). All these parameters indicate optimum crystalline perfection at around 820 °C. The degradation of  $T_c$  at above 820 °C is likely related to minor inter-reaction of the liquid with the substrate for the higher liquid fraction, *cf.* 820 °C.

[S1]

Tair F., Melting temperature of  $YBa_2Cu_3O_{7-x}$  and  $GdBa_2Cu_3O_{7-x}$  at subatmospheric partial pressure, *J. Alloys Compd.*, **692**, 6, pp. 789-792, 2017  
<https://doi.org/10.1016/j.jallcom.2016.08.072>

[S2]

Kursumovic A. et al., Study of the rate-limiting processes in liquid-phase epitaxy of thick YBaCuO films, *J. Cryst. Growth.*, **218**, 1, pp.45-56, 2000  
[https://doi.org/10.1016/S0022-0248\(00\)00519-4](https://doi.org/10.1016/S0022-0248(00)00519-4)

[S3]

Erb A. et al.,  $Ba_2Cu_3O_{7-\delta}$ -BaCuO<sub>2</sub>-CuO: investigations on the phase diagram and growth of single crystals I. The system BaCuO<sub>2</sub>-CuO<sub>x</sub>, *J. Cryst. Growth.*, **132**, 3, 1993  
[https://doi.org/10.1016/0022-0248\(93\)90063-3](https://doi.org/10.1016/0022-0248(93)90063-3)

[S4]

Chow J. C. L. et al., SmBa<sub>2</sub>Cu<sub>3</sub>O<sub>6.5</sub> seed fabrication for seeded peritectic solidification of YBa<sub>2</sub>Cu<sub>3</sub>O<sub>7- $\delta$</sub> , *J. Mater. Sci.*, **33**, pp. 133-137, 1998  
<https://doi.org/10.1023/A:1004353915075>

[S5]

Zhou Y. et al., Melting and solidification of  $Y_{1-x}Yb_xBa_2Cu_3O_y$ : Influences of Yb doping and oxygen partial pressure, *Physica C*, **341**, 4, pp2475-2476, 2000  
[https://doi.org/10.1016/S0921-4534\(00\)01196-5](https://doi.org/10.1016/S0921-4534(00)01196-5)

[S6]

Paulose K.V. et al., YBa<sub>2</sub>NbO<sub>6</sub>: synthesis, properties and compatibility with YBa<sub>2</sub>Cu<sub>3</sub>O<sub>7-δ</sub>, *Physica C*, **193**, 3, pp 273-276, 1992  
[https://doi.org/10.1016/0921-4534\(92\)90728-U](https://doi.org/10.1016/0921-4534(92)90728-U)